



CHORUS

This is the accepted manuscript made available via CHORUS. The article has been published as:

Enhancement of charge density wave correlations in a Holstein model with an anharmonic phonon potential

C. Kvande, C. Feng, F. Hébert, G. G. Batrouni, and R. T. Scalettar

Phys. Rev. B **108**, 075119 — Published 7 August 2023

DOI: [10.1103/PhysRevB.108.075119](https://doi.org/10.1103/PhysRevB.108.075119)

Enhancement of Charge Density Wave Correlations in a Holstein Model with an Anharmonic Phonon Potential

C. Kvande,^{1,2,*} C. Feng,^{3,2} F. Hébert,⁴ G. G. Batrouni,^{5,6,4} and R. T. Scalettar²

¹*Physics Department, Kalamazoo College, 1200 Academy Street, Kalamazoo, Michigan, 49006-3295 USA*

²*Department of Physics, University of California, Davis, California 95616, USA*

³*Center for Computational Quantum Physics, Flatiron Institute, 162 Fifth Avenue, New York, New York 10010*

⁴*Université Côte d'Azur, CNRS, INPHYNI, France*

⁵*Department of Physics, National University of Singapore, 2 Science Drive 3, 117551 Singapore*

⁶*Centre for Quantum Technologies, National University of Singapore; 2 Science Drive 3, 117543 Singapore*

The Holstein Hamiltonian describes itinerant electrons whose site density couples to local phonon degrees of freedom. In the single site limit, at half-filling, the electron-phonon coupling results in a double well structure for the lattice displacement, favoring empty or doubly occupied sites. In two dimensions, and on a bipartite lattice in $d \geq 2$, an intersite hopping causes these doubly occupied and empty sites to alternate in a charge density wave (CDW) pattern when the temperature is lowered. Because a discrete symmetry is broken, this occurs in a conventional second-order transition at finite T_{cdw} . In this paper, we investigate the effect of changing the phonon potential energy to one with an *intrinsic* double well structure even in the absence of an electron-phonon coupling. While this aids in the initial process of pair formation, the implications for subsequent CDW order are non-trivial. One expects that, when the electron-phonon coupling is too strong, the double wells become deep and the polaron mass large, an effect which *reduces* T_{cdw} . We show here the existence of regions of parameter space where the double well potential, while aiding local pair formation, does so in a way which also substantially enhances long range CDW order.

PACS numbers: 71.10.Hf, 71.30.+h, 71.45.Lr, 63.20.-e

I. INTRODUCTION

The Holstein Hamiltonian¹ provides a simplified description of the interactions between electron and phonon degrees of freedom in a solid, including polaron and bipolaron formation,²⁻¹⁰ and the origin of low temperature phases with diagonal charge density wave (CDW) or off-diagonal superconducting (SC) long range order.¹¹⁻²¹ Although the electron-phonon (el-ph) interaction, λ , initiates these phases, its effect is non-monotonic.^{19,22-28} Quantum Monte Carlo (QMC) simulations show that pairs become heavy and CDW and SC transition temperatures go to zero at strong coupling λ .²⁹ This finding is in contrast with the approximate Eliashberg theory, which predicts that T_{cdw} increases monotonically with λ , and provides a challenge to achieving high CDW transition temperatures.

As a consequence, the search for situations in which large λ does not reduce the tendency for long range order has been an ongoing focus of recent analytic and numerical studies. For example, in the case of SC, it has been suggested that a Su-Schrieffer-Heeger (SSH) interaction³⁰⁻³³ might avoid the problem of large effective mass.^{34,35} Elevated CDW transitions have also been found in studies of the SSH model on a 3D Lieb lattice appropriate to the bismuthates.³⁶

In infinite dimension, using a technique similar to dynamical mean field theory (DMFT), Freericks, Jarrell, and Mahan³⁷ studied the effects of a simple anharmonic term in the form of an additional quartic potential energy for the phonons. They concluded that a CDW phase exists for a large range of densities at low anharmonicity,

but that the CDW is gradually replaced at low and high densities by a SC phase as the anharmonicity increases. The half-filled system always remains in a CDW state. They also observed a decrease of the critical temperatures at which CDW and SC phases appear with increasing anharmonicity. Similar models have been studied in one dimension.³⁸

In this manuscript we consider a route to high CDW transition temperatures driven by a double well (anharmonic) phonon potential resulting from *negative* quadratic, and positive quartic, terms in the displacement. Such a potential favors the development of a pre-existing non zero phonon field, without the mediation of electron-phonon coupling, and then favors electron occupations to organize into empty and doubly occupied sites when the el-ph interaction is present. A number of previous studies of anharmonicity with *positive* quadratic and positive quartic phonon potential energy terms,^{13,37-47} have in general found a suppression of charge order at half-filling, in agreement with the DMFT study noted above. Nonlinearities in the coupling terms between fermions and phonons³⁹⁻⁴² have led to similar conclusions. This existing literature brings into focus our key result: anharmonicity can produce an enhancement of T_{cdw} if it occurs in the form of an intrinsic double well potential.

There are a number of experimental motivations for considering such a generalization of the Holstein Hamiltonian. One is to understand Kondo/heavy fermion physics in materials like $\text{SmOs}_4\text{Sb}_{12}$. Most typically, heavy fermion behavior arises due to the interaction of conduction electrons with *magnetic* degrees of freedom (local

moments). However, it has been suggested, even dating back to Kondo,⁴⁸ that other two level systems might cause similar phenomena. In the case of $\text{SmOs}_4\text{Sb}_{12}$ a large applied magnetic field, which would quench fluctuations of local magnetic moments and hence of Kondo physics, does not destroy the heavy fermion behavior. It has been suggested, then, that rather than conduction electrons interacting with local $S = 1/2$ spins, it is instead the coupling to two level phonon degrees of freedom that is relevant.^{49,50}

The remainder of this paper is organized as follows: We first define the model, its parameters and physical observables, and then give a brief summary of our two, complementary, QMC techniques. Results are then shown for local observables and for charge structure factors for different forms of the anharmonic potential using energy scales close to those typically chosen in the conventional Holstein model. Finite size scaling (FSS) is employed to extract T_{cdw} . Similar calculations are then done for parameters which fix the average phonon displacement in order to demonstrate that the enhanced CDW T_{cdw} is not a ‘trivial’ effect associated with artificially large displacements. A conclusion summarizes our work and points to possible future directions, and is followed by Appendices containing further details of our model and simulations.

II. MODEL AND METHODS

We consider the Hamiltonian,

$$\begin{aligned}
H = & -t \sum_{\langle \vec{i}, \vec{j} \rangle \sigma} (c_{i\sigma}^\dagger c_{j\sigma} + h.c.) - \mu \sum_{\vec{i}\sigma} n_{i\sigma} \\
& + \sum_{\vec{i}} \left(-Ax_i^2 + Bx_i^4 + \frac{p_i^2}{2m} \right) \\
& + \lambda \sum_{\vec{i}} x_i (n_{i\uparrow} + n_{i\downarrow} - 1) \quad (1)
\end{aligned}$$

The sums run over the $N = L^2$ sites of a two-dimensional square lattice with periodic boundary conditions. The operator $c_{i\sigma}$ ($c_{i\sigma}^\dagger$) destroys (creates) a fermion of spin $\sigma = \uparrow$ or \downarrow on site $\vec{i} = (i_x, i_y)$; $n_{i\sigma} = c_{i\sigma}^\dagger c_{i\sigma}$ is the corresponding number operator; x_i and p_i are the canonically conjugate displacement and momentum operators of the phonon mode at site \vec{i} . The first line of Eq. 1 represents the hopping energy of the fermions between neighboring sites $\langle \vec{i}, \vec{j} \rangle$. A chemical potential term is included to emphasize our algorithms perform simulations in the grand canonical ensemble. The hopping parameter t will be used as the energy scale. The second line in Eq. 1 represents the energy of the phonons of quadratic potential $-Ax_i^2$ and anharmonic term Bx_i^4 . This form, with a negative quadratic term (i.e. $A > 0$), results in a double well. Without loss of generality, we set $m = 1$. The third line in Eq. 1 is the phonon-electron interaction, written in a

particle hole symmetric (PHS) form so that $\mu = 0$ corresponds to half-filling. A further discussion of this PHS appears in Appendix 1. The PHS also ensures the values of displacement x corresponding to empty and doubly occupied sites are symmetrically located about the origin $x = 0$.

In order to connect to previous QMC studies of the conventional Holstein Hamiltonian,¹ where there is only a positive quadratic term in the phonon displacement with phonon frequency ω_0 , we note that one would express the quadratic coefficient in terms of the frequency, as $A = m\omega_0^2/2$. In that situation, ω_0 also enters the re-writing of the electron-phonon interaction in terms of phonon creation (destruction) operators, $a_{i\tau}^\dagger(a_{i\tau})$: $\lambda \sum_{\vec{i}} x_i (n_{i\uparrow} + n_{i\downarrow} - 1) = g \sum_{\vec{i}} (a_{i\tau} + a_{i\tau}^\dagger) (n_{i\uparrow} + n_{i\downarrow} - 1)$ with $g = \lambda/\sqrt{2\omega_0}$ where $\omega_0 = \sqrt{2A}$. To compare with previous work on the conventional Holstein model, we then choose a commonly used value of coupling g , keep B fixed to a small value and vary A to explore different depths of the potential wells. The values of A are chosen to keep $\omega_0 = \sqrt{2A}$ and $\lambda = g\sqrt{2\omega_0}$ of order unity, in the range of values that are typically used for the conventional Holstein model. Results corresponding to this choice of parameters will be presented in Sec. III.

However, although analogous values of the el-ph coupling and phonon frequency are used in this comparison, the anharmonic form of the full phonon potential leads to displacements which are different in magnitude from the simplest harmonic situation. One can ensure that the coupling to the electrons, which combines λ and x_i , is equivalent in magnitude to the conventional Holstein case by choosing parameters A and B which are tuned to keep the average phonon displacement fixed at a certain value x_0 , where x_0 is given by λ/ω_0^2 in the conventional Holstein case. This is accomplished through the choice $A = (4Bx_0^3 - \lambda)/(2x_0)$, a relation derived in Appendix 2; results corresponding to this choice of parameters will be presented in Sec. IV.

We employ two methods to study Eq. 1. The first is Determinant Quantum Monte Carlo (DQMC).⁵¹ In this approach, the action for the phonon degrees of freedom at inverse temperature (imaginary time) β is expressed as a path-integral over a space-imaginary time grid, and the fermionic degrees of freedom, which appear only quadratically in Eq. 1, are integrated out analytically. The resulting partition function consists of an integral over the phonon field $x_i(\tau)$ which is performed stochastically. The weight for phonon field configurations takes the form of the square of the determinant of a matrix (the fermionic traces over spin up and down yield identical determinants) whose dimension is the number of spatial sites N . Consequently, there is no sign problem. However, a sweep through the space-time lattice scales as $N^3\beta$, and possibly as $N^3\beta^2$, depending on the degree to which numerical instabilities require more accurate (numerically stable) treatment of the linear algebra.

DQMC studies of the conventional Holstein model

date back to the same period as for the Hubbard model^{14,16,52–54} but precise quantitative values for T_{cdw} have emerged only more recently e.g. on square,²³ honeycomb²⁴ and cubic lattices.²⁸ The delay in computing the transition temperature partly originated in the quantum simulation community's focus instead on electron-electron interactions as driving exotic superconductivity in the cuprates, but also because of the significant computational challenge of very long autocorrelation times. In DQMC simulations of the Hubbard model, updates of the Hubbard-Stratonovich field at a single space-time point decorrelate very rapidly (a few sweeps of the lattice). However, in DQMC for the Holstein model, autocorrelation times are instead often hundreds or thousands of sweeps.

This bottleneck has led to the development of QMC methods for electron-phonon Hamiltonians based on a Langevin update of the entire space-time lattice.^{28,55–58} Such approaches can be formulated in a way which scales linearly in N (albeit with a smaller step size for each move than in DQMC) via the replacement of the determinant by an integration over a pseudofermion field. Equally important to this linear scaling, Fourier acceleration methods^{55,59} can be employed to reduce autocorrelation times dramatically. Quantitative details of DQMC and Langevin methods are discussed in Appendix 3. Alternate methods to address long autocorrelation times use machine-learning approaches⁶⁰ and Wang-Landau sampling.⁶¹

We will employ both DQMC and Langevin methods here. Most of the simulations have been performed with DQMC and the results presented here were obtained with this method unless otherwise indicated in the figures. In certain key cases, results have been confirmed by comparing DQMC and Langevin simulations.

The most simple observable we study is the density, $n = \sum_{\vec{i}} \langle n_{\vec{i}\sigma} \rangle / L^2$, and its behavior as a function of μ . A plateau in $n(\mu)$ signals a vanishing compressibility, $\kappa = \partial n / \partial \mu$, and the presence of a charge gap Δ . As noted earlier, the PHS form of the Hamiltonian ensures half-filling $n = 1$ corresponds to $\mu = 0$. This is the optimal density for a CDW phase, since it allows a precise alternation of doubly occupied and empty sites.

We will also examine other local quantities such as the average value of the phonon displacement $\langle x_{\vec{i}} \rangle$, the double occupancy $D = \langle n_{\vec{i}\uparrow} n_{\vec{i}\downarrow} \rangle$, and the x component of the kinetic energy $K = \langle c_{\vec{i},\sigma}^\dagger c_{\vec{i}+\hat{x},\sigma} + h.c. \rangle$.

To characterize further the presence of a (long range) CDW phase, we study the charge structure factor, the Fourier transform at momentum (π, π) of the density-density correlation function,

$$S_{\text{cdw}} = \frac{1}{N} \sum_{\vec{i}, \vec{j}} \langle n_{\vec{i}} n_{\vec{i}+\vec{j}} \rangle (-1)^{j_x+j_y}. \quad (2)$$

Here $n_{\vec{i}} = n_{\vec{i}\uparrow} + n_{\vec{i}\downarrow}$ is the number of fermions on site \vec{i} . In a phase with short range order, $\langle n_{\vec{i}} n_{\vec{i}+\vec{j}} \rangle$ will decay

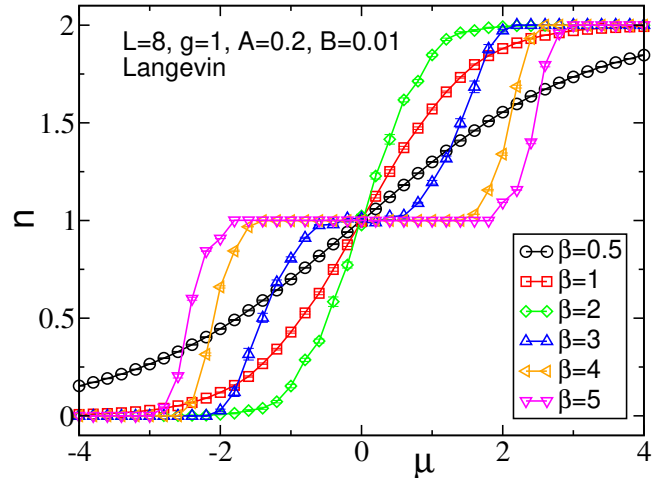


FIG. 1. (Color online). Density, n , as a function of chemical potential, μ , for $g = 1$, $B = 0.01$ and $A = 0.2$. $\lambda = \sqrt{2}\omega_0 g$ with $\omega_0 = \sqrt{2A}$. At high temperature T , n deviates immediately from half-filling as μ is changed from $\mu = 0$. However, as T decreases a plateau in $n(\mu)$ develops: the density is frozen at half-filling until $|\mu|$ exceeds a critical threshold, half the single particle gap Δ . This gap formation around $\beta \simeq 3$ is an indication of the entry into the ordered CDW phase at low T . The simulations were performed only for $\mu \geq 0$ since the system is particle-hole symmetric.

rapidly to zero as the separation $|\vec{j}|$ increases. Thus in the sum over all sites \vec{i} and separations \vec{j} in Eq. 2, the only sizeable contributions come from small separations \vec{j} , and the double sum is of order N . The division by N then implies $S_{\text{cdw}} \sim O(1)$, i.e. is independent of lattice size. In a phase with long range order, on the other hand, the double sum is $O(N^2)$ and $S_{\text{cdw}} \sim O(N)$ (i.e. is extensive) after normalization. The optimal ordering vector \vec{q} for a half-filled square lattice is at $\vec{q} = (\pi, \pi)$ owing to the perfect nesting at this momentum. Incommensurate order at $\vec{q} \neq (\pi, \pi)$ is possible upon doping, but we do not see evidence of it here.

III. SIMULATIONS FOR CANONICAL PARAMETERS

We first show results for values of Hamiltonian parameters similar to those used in past studies of the conventional Holstein Hamiltonian in order to facilitate comparison of our results with those in the literature. Specifically, we fix the electron-phonon coupling $g \sum_{\vec{i}} (a_{\vec{i}} + a_{\vec{i}}^\dagger) (n_{\vec{i}\uparrow} + n_{\vec{i}\downarrow} - 1)$ at $g = 1$, and pick $A = 0.1, 0.2, 0.5$. These correspond to quadratic potential curvatures $\omega_0^2/2$ with $\omega_0 = \sqrt{2A} = 0.44, 0.63, 1.00$, similar to the commonly used values $\omega_0 = 0.5 - 2.0$.^{19,22–28,40,41} When expressed in terms of a coupling of fermionic density to lattice displacement, $\lambda = \sqrt{2}\omega_0 g = 0.94, 1.12, 1.41$, again in

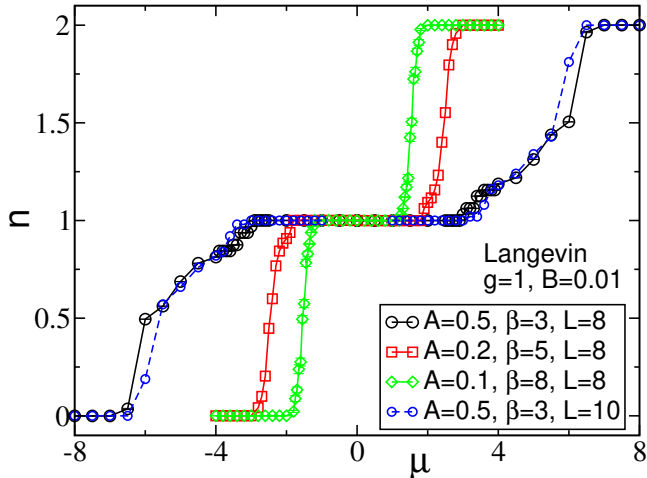


FIG. 2. (Color online). Density, n , as a function of chemical potential, μ , for $g = 1$, $B = 0.01$ and several values of A with $\lambda = \sqrt{2\omega_0}g$ and $\omega_0 = \sqrt{2A}$. β is chosen so that $n(\mu)$ no longer changes with further lowering of the temperature allowing the simulation to pick up only ground state properties. (See also Fig. 6.) We observe a decrease of the charge gap as A decreases from 0.5 to 0.1. For the $A = 0.5$ case, a comparison of results for $L = 8$ and $L = 10$ shows that the width of the gap does not change significantly with size.

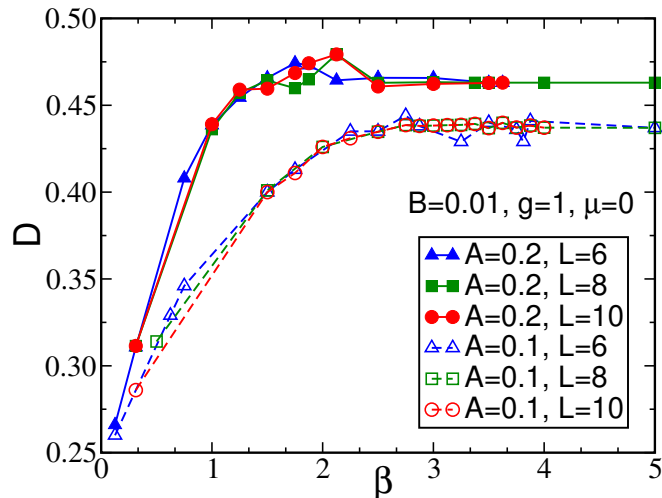


FIG. 3. (Color online). The double occupancy, D , as a function of β for $B = 0.01$, $\mu = 0$, $g = 1$, for different sizes L , and for two different choices of A : $A = 0.1$ (open symbols, dashed lines) and $A = 0.2$ (filled symbols, solid lines). $\lambda = \sqrt{2\omega_0}g$ with $\omega_0 = \sqrt{2A}$. D saturates to a larger value and at a higher temperature for $A = 0.2$, compared to $A = 0.1$.

the usual range of $\lambda \sim 1$.

A. Local Observables

Phases with long range order are typically characterized by gaps in their single particle excitation spectra. As noted earlier, such gaps are most simply revealed via a vanishing of the compressibility $\kappa = \partial n / \partial \mu$, i.e. by a plateau in a plot of n versus μ . In Fig. 1 we fix $A = 0.2$, $B = 0.01$, $g = 1$. At high temperatures the compressibility at half-filling ($\mu = 0$) is finite. However, when $T \lesssim t/3$ the slope of $n(\mu = 0)$ becomes small. At $T = t/5$, n remains fixed at $n \sim 1$ until μ exceeds $\mu \sim 2t$, indicating a CDW gap $\Delta \sim 4t$. The non-monotonic evolution of the compressibility in Fig. 1 can be understood by the fact that, in addition to the non-trivial physics of CDW formation which causes $\kappa \sim 0$ at low T , in the limit of very high temperature the compressibility must also become small, i.e. $\kappa \sim 1/T$.

Figure 2 generalizes Fig. 1 to several distinct values of A . As explained before, for each A , the electron-phonon coupling is chosen to mimic the procedure in the usual Holstein model, namely by identifying the frequency corresponding to the curvature, $\omega_0 = \sqrt{2A}$, and then determining the electron-phonon coupling $\lambda = \sqrt{2\omega_0}g$ with g fixed at $g = 1$. Figure 2 allows us to assess how the single particle gap Δ is affected by the (negative) quadratic phonon curvature. We find that Δ increases with increasing A . We will return to this point in discussing the effect of varying A on the CDW transition temperature.

We comment that for $A = 0.5$, one can see additional steps in n above half-filling. For $L = 8$ ($N = 64$), these occur at integer densities corresponding to even numbers of particles $N_\uparrow + N_\downarrow = 66, 68, \dots$ on the lattice and reflect the tendency to add particles in $\uparrow\downarrow$ pairs due to the attractive interaction mediated by the phonons. Similar steps are evident for $L = 10$. This is an effect seen also in QMC simulations of the conventional Holstein model.

The double occupancy D is given in Fig. 3 for two values of A and different lattice sizes $L = 6, 8, 10$. D evolves rapidly from its high temperature (uncorrelated) value $D = \langle n_{\uparrow} n_{\downarrow} \rangle \sim \langle n_{\uparrow} \rangle \langle n_{\downarrow} \rangle \sim 1/4$ as T decreases, reflecting the fact that pair formation precedes the ordering of pairs into a CDW pattern. The weak feature in D at $\beta \sim 2$ will be seen to coincide with CDW formation.

A final local observable is the kinetic energy K , given in Fig. 4. K first evolves from its particle-hole symmetric high temperature limit $K = 0$, to negative values as lower energy states dominate. This steady decrease is interrupted by upturns in K (decreases in the magnitude of hopping). These local maxima correlate with the CDW ordering transitions. See below.

B. Long Range Charge Order

Two final observables directly probe charge order. The first, shown in the top panel of Fig. 5, is the real space density-density correlation function $\langle n_{\vec{i}} n_{\vec{i}+\vec{j}} \rangle$. At $\beta = 1$ these differ from their $\lambda = 0$ values $\langle n_{\vec{i}} n_{\vec{i}+\vec{j}} \rangle =$

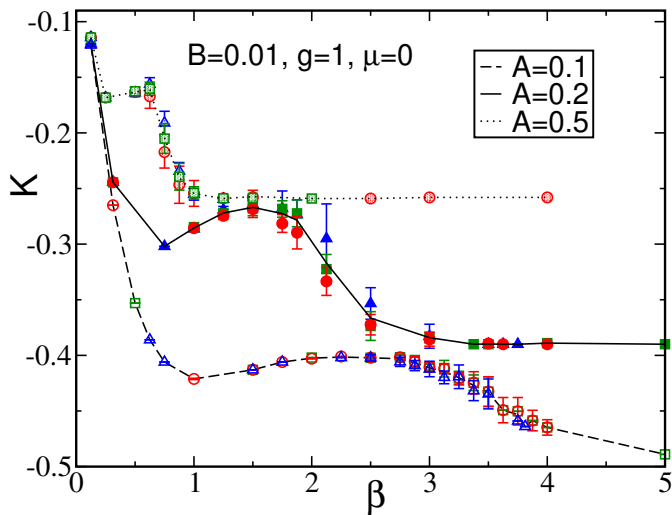


FIG. 4. (Color online). K , the x component of kinetic energy, as a function of inverse temperature for different values of $A = 0.1, 0.2$ and 0.5 and different sizes $L = 6, 8$ and 10 . All data have $B = 0.01$, $\mu = 0$, $g = 1$. $\lambda = \sqrt{2\omega_0 g}$ with $\omega_0 = \sqrt{2A}$. Red circles are $L = 10$, green squares $L = 8$, and blue triangles are $L = 6$. The lines show the average over the different lattice sizes at each point. Because of particle-hole symmetry, the high temperature (small β) value of K vanishes: The non interacting energy levels $\epsilon(\mathbf{k})$ are symmetric around $\epsilon = 0$ and, at high T , all levels are occupied equally. As β increases, the $\epsilon < 0$ states are preferentially occupied, and $K < 0$.

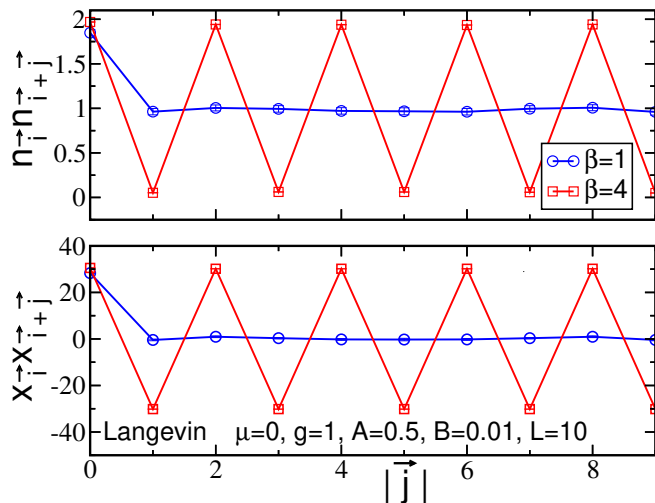


FIG. 5. (Color online). Density-density $\langle n_{\vec{i}} n_{\vec{i}+\vec{j}} \rangle$ and phonon displacement correlations $\langle x_{\vec{i}} x_{\vec{i}+\vec{j}} \rangle$ correlators along the side of the square lattice at high ($\beta = 1$) and low ($\beta = 4$) temperatures at $\mu = 0$ (half-filling). As β increases the system goes from an unordered phase to a charge density wave phase where an order develop in both the charge density and phonon displacements. One should notice that, for $\vec{j} = \vec{0}$, due to the double well potential, $\langle x_{\vec{i}} x_{\vec{i}} \rangle$ is sizeable even in the high temperature phase.

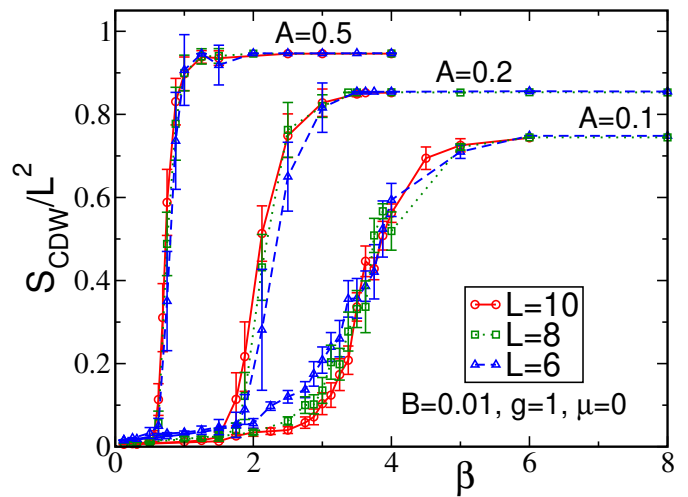


FIG. 6. (Color online). Evolution of the charge structure factor S_{cdw} with inverse temperature. Here $B = 0.01$, $\mu = 0$, and $g = 1$. From left to right, we have $A = 0.5$, $A = 0.2$, and $A = 0.1$ with corresponding $\omega_0 = \sqrt{2A}$ and $\lambda = \sqrt{2\omega_0 g}$. As A increases, the structure factor S_{cdw} saturates at a larger value and the transition occurs at a larger temperature.

$\langle n_{\vec{i}} \rangle \langle n_{\vec{i}+\vec{j}} \rangle = 1$ only on-site, $\vec{i} = \vec{j}$. That is, pairs have formed locally, but not yet ordered between different sites. However, at $\beta = 4$ the oscillating, and non-decaying, pattern indicates long range CDW formation. Figure 6 exhibits the Fourier transform of Eq.2, i.e. the structure factor S_{cdw} . An additional normalization to $N = L^2$ is performed, so that $S_{\text{cdw}}/N \propto 1/N$ at small β , and $S_{\text{cdw}}/N \propto 1$ at large β . An abrupt change indicates the CDW transition. The invariance of the low T value across different lattice sizes is another illustration the order is long-ranged.

The positions of these steps are close to the locations of the local minima in the absolute value of the kinetic energy K in Fig. 4. We interpret this to indicate that the preferential occupation of bands with $\epsilon(\mathbf{k}) < 0$, which occurs even in the non-interacting limit as T is lowered, gets interrupted by the CDW formation.

The bottom panel of Fig. 5 indicates that the alternating pattern in the fermionic density is accompanied by an alternating pattern in the phonon displacements.

The key features, however, of Fig. 6 are the *high values of the transition temperatures* T_{cdw} for the larger values of A where the double well phonon potential energy favors non-zero displacements. Typical values of T_{cdw} in the conventional Holstein model are in the range $T_{\text{cdw}}/t \sim 0.2 - 0.3$ for analogous choices of g and ω_0 .²⁵ In the next section, we verify that these high T_{cdw} persist even when the product of the electron-phonon coupling and typical phonon displacements are restricted to be the same as in the conventional Holstein model.

We conclude this discussion by presenting a scaling analysis to determine T_{cdw} more precisely. When nor-

malized by $N^{-1} = L^{-2}$, a lattice-size independent structure factor provides evidence for ground state long range order, as already seen in Fig. 6. The temperature at which this order first occurs can be determined by examining $L^{-\gamma/\nu} S_{\text{cdw}}$. The theory of finite size scaling predicts that curves of $L^{-\gamma/\nu} S_{\text{cdw}}$ as functions of T (or β) for different lattice sizes should all cross at one point, thus yielding the value of T_{cdw} . Here in the Holstein model on a square lattice, the transition is in the 2D Ising universality class with $\gamma/\nu = 7/4$, simplifying the analysis. Figure 7 shows the result for the two cases with $A = 0.1$ (top) and $A = 0.5$ (bottom). The crossing is at $T_{\text{cdw}} = 0.29 \pm 0.02$ ($\beta_{\text{cdw}} = 3.5 \pm 0.2$) for $A = 0.1$ and as high as $T_{\text{cdw}} = 1.8 \pm 0.2$ ($\beta_{\text{cdw}} = 0.56 \pm 0.06$) for $A = 0.5$.

We also demonstrate that the two computational methods, DQMC and Langevin, give consistent results by comparing results for $L = 8$ in the insets of Fig. 7.

IV. SIMULATIONS AT FIXED AVERAGE PHONON DISPLACEMENT

In the preceding section we reported values for T_{cdw}/t which exceed by a factor of two or three those obtained over a range of values of electron-phonon couplings λ and phonon frequencies ω_0 previously reported for the conventional Holstein Hamiltonian.

These results are already significant because the existence of a maximal T_{cdw}/t at intermediate λ and ω_0 suggests a fundamental limit to the CDW transition temperature in the conventional Holstein model. However, one could still ask whether the high critical transition temperatures of Fig. 6 are associated with anomalously large phonon displacements, or some related unphysical parameter choice. In this section we reproduce many of the preceding results tuning the anharmonic potential (that is, A and B) to keep fixed phonon displacement. More specifically, we show in Appendix B that the choice

$$A = \frac{4Bx_0^3 - \lambda}{2x_0} \quad (3)$$

keeps $\langle x \rangle = x_0$. Thus when we vary A we do so with an accompanying change in B to fix the mean phonon displacement. We chose to compare to the conventional Holstein model with $\lambda = 2$ and $\omega_0 = 1$ for which $x_0 = \langle x \rangle = \lambda/\omega_0^2 = 2$. In addition, we use the same value of $\lambda = 2$ in both models to keep the product λx similar. We studied two cases with $B = 0.1$ and $B = 0.2$ which give $A = 0.3$ and $A = 1.1$, respectively.

A. Local Observables

To ensure the observation of high CDW transition temperatures reported in the preceding section is robust, we focus here on measurements of long range order which more precisely determine T_{cdw} . Nevertheless, it is useful to examine one local measurement, the kinetic energy,

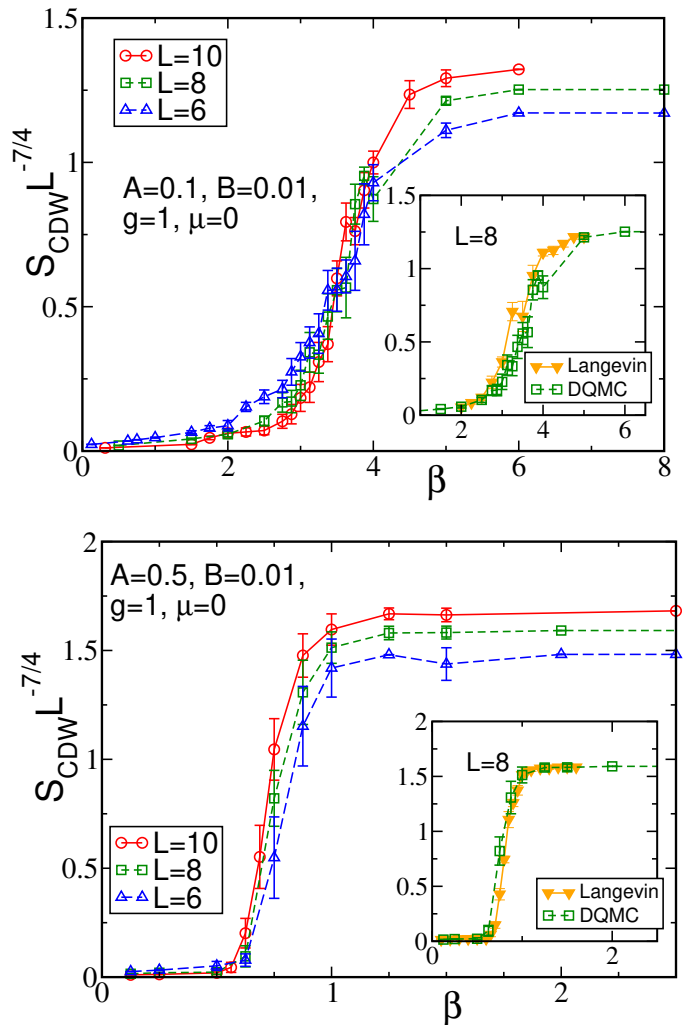


FIG. 7. (Color online). Scaling analysis of the charge structure factor for $B = 0.01$, $g = 1$, $\mu = 0$ and $A = 0.1$ (top) or $A = 0.5$ (bottom) with corresponding $\omega_0 = \sqrt{2A}$ and $\lambda = \sqrt{2\omega_0 g}$. When S_{cdw} is normalized by $L^{\gamma/\nu}$ with $\gamma/\nu = 7/4$, the 2D Ising values, a crossing as a function of inverse temperature β occurs at the critical point. The top figure shows the $A = 0.1$ case for which we observe the crossing around $\beta_{\text{cdw}} = 3.5 \pm 0.2$. In the bottom figure, $A = 0.5$ and $\beta_{\text{cdw}} = 0.56 \pm 0.06$. The insets show a comparison between results obtained with DQMC and Langevin methods for $L = 8$ in the critical region.

since its non-monotonic behavior has been seen earlier to provide an important initial indication of the onset of the insulating CDW phase. Figure 8 exhibits this decrease in magnitude of K in the vicinity of the CDW ordering transition.

B. Long Range Charge Order

Figure 9 shows a finite size scaling crossing plot for ~~one of~~ these ‘fair comparisons’ in which the phonon dis-

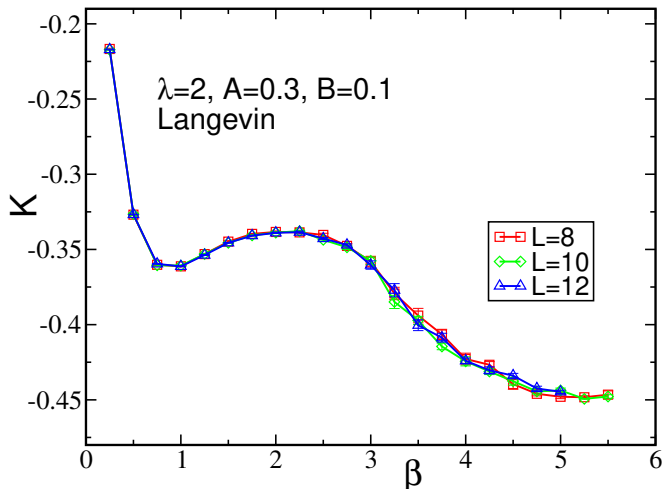


FIG. 8. (Color online). Kinetic energy as a function of β . The non-monotonic behavior of the kinetic energy reflects the development of charge correlations. Parameters are $A = 0.3$, $B = 0.1$, $\lambda = 2$ and have been chosen to obtain a phonon field $x_0 = 2$.

placement is restricted to be the same as for the conventional Holstein model. We find $\beta_{\text{cdw}} \sim 3.25$ ($T_{\text{cdw}} \sim 0.31$), which is higher than the transition temperature of the Holstein model on a half-filled square lattice with $\lambda = 2, \omega_0 = 1$.²⁶ Choosing $A = 1.1$ and $B = 0.2$ and keeping $\lambda = 2, \omega_0 = 1$ and $x_0 = 2$, we increase the transition temperature to $\beta_{\text{cdw}} = 2.5$. This shows that for the same fixed average value of lattice displacement, x_0 , we obtain higher critical temperatures by increasing A and B . Furthermore, as noted earlier, T_{cdw} as a function of λ in the Holstein model is non-monotonic, with a maximum $T_{\text{cdw}} \sim 0.25$ at dimensionless electron-phonon coupling strength $\lambda_D \sim 0.4$ when $\omega_0 = 1$.²⁶ Meanwhile, the transition temperature does not depend on ω_0 sensitively as long as the effective attraction in the Holstein model $U = -\lambda^2/\omega_0^2$ is fixed.⁵⁸ The large $T_{\text{cdw}} \sim 2$ shown in Fig. 7 (bottom), much higher than the maximum T_{cdw} we can achieve in the pure Holstein model, indicates the Holstein model with anharmonic potential we study here significantly increases the CDW phase transition temperature.

V. CONCLUSIONS

In this paper we have used determinant Quantum Monte Carlo and Langevin simulations to examine the properties of a square lattice Holstein model with an anharmonic phonon potential. This potential has an intrinsic double well structure favoring non zero phonons fields and, consequently, empty and doubly occupied sites. Unlike most previous extensions of the Holstein model to

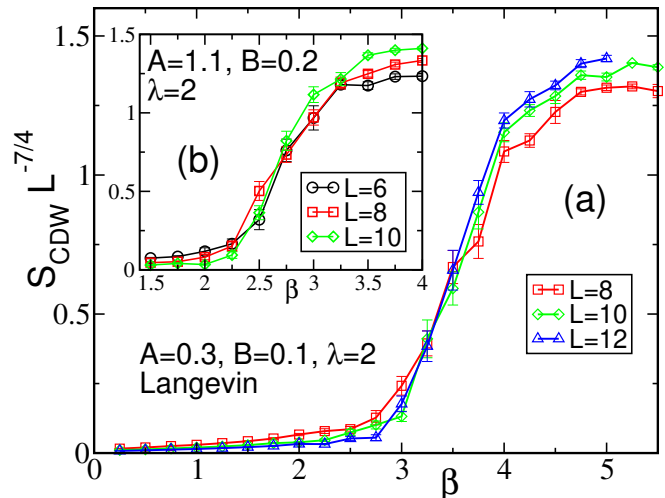


FIG. 9. (Color online). Langevin data for the rescaled structure factor $S_{\text{cdw}} L^{-7/4}$ for (a) $A = 0.3, B = 0.1, \lambda = 2$ and (b, inset) $A = 1.1, B = 0.2, \lambda = 2$. Both cases correspond to a phonon field $x_0 = 2$. A crossing at $\beta_{\text{cdw}} \sim 3.25$ (a) gives the position of the CDW transition for $A = 0.3$ and $B = 0.1$, whereas the transition is shifted towards $\beta_{\text{cdw}} \sim 2.5$ for $A = 1.1$ and $B = 0.2$ (b). One should notice that our simulations are limited to $L = 10$ for the second case.

include anharmonicity, our results show a marked increase in the CDW transition temperatures, from $T_{\text{cdw}} \sim t/6 - t/4$ for the conventional Holstein model, to $T_{\text{cdw}} \sim t/2 - t$. Our result is not a consequence of a trivial rescaling of T_{cdw} resulting from larger phonon displacements; we demonstrated this by choosing parameter sets where the average phonon displacement is similar to those in the conventional Holstein model. In any case, in the Holstein-Hubbard model, T_{cdw} has a maximum as a function of electron-phonon coupling, phonon frequency, and the resulting phonon displacement, which is well below the transition temperatures found here.

It would be interesting to explore superconducting correlations in this model. One expects CDW and SC to be competitive, so that the emergence of SC will surely require doping away from half-filling. QMC is especially useful here especially given the uncertainty in how to include anharmonicity⁴⁶ in analytic approaches like Migdal-Eliashberg theory,^{62,63} which have been central to the understanding of the conventional Holstein Hamiltonian.^{29,42,64,65} Progress has been made in that method by generalizing the single phonon spectral density.⁴⁶

Although we have mainly characterized our CDW phase as one in which the electron density is modulated, there is an accompanying alternation of phonon coordinates in our model, as seen in the bottom panel of Fig. 5. Since our phonon degrees of freedom are not directly coupled to each other, this oscillating structure forms via coupling to the conduction electrons. This effect is similar to that occurring in the dense limit of the Kondo

Lattice (KL) model^{66–68} in which local moments which have no direct coupling can nevertheless order antiferromagnetically via an indirect Ruderman-Kittel-Kasuya-Yosida (RKKY)^{69–71} interaction mediated by conduction electrons.

A potentially interesting application of the use of QMC to compute the properties of anharmonic electron-phonon systems is to study the physics of “rattlers” for high figure-of-merit thermoelectric materials, and specifically to the thermal conductivity.^{72,73}

ACKNOWLEDGMENTS

The work of RTS was supported by the grant DE-SC0014671 funded by the U.S. Department of Energy, Office of Science. CK’s work was supported by the UC Davis Physics REU program under NSF grant PHY2150515.

Appendix 1: Particle-Hole Symmetry in the presence of an Anharmonic Potential

There are two related ways to discuss the particle-hole symmetry of the model. As the one particle band due to the kinetic term is symmetric around $\mu = 0$, the first way is to consider a single site model (that is, $t = 0$) with the phonon potential of Eq. 1,

$$V(x) = -Ax^2 + Bx^4 + \lambda x(n - 1) - \mu n, \quad (4)$$

and to show it has a similar particle-hole symmetry.

The average density is given by,

$$\begin{aligned} \langle n_{\uparrow} \rangle &= Z^{-1} \sum_{n_{\uparrow}=0}^1 \sum_{n_{\downarrow}=0}^1 \int dx n_{\uparrow} e^{-\beta V(x)} \\ Z &= \sum_{n_{\uparrow}=0}^1 \sum_{n_{\downarrow}=0}^1 \int dx e^{-\beta V(x)} \end{aligned} \quad (5)$$

If we introduce the notation $I(n_{\uparrow}, n_{\downarrow})$ to denote the integral for a specific choice of number operators, we can re-write Eqn. 5 as:

$$\langle n_{\uparrow} \rangle = \frac{I(1, 0) + I(1, 1)}{I(0, 0) + 2I(1, 0) + I(1, 1)} \quad (6)$$

where the denominator is the partition function. Rearranging this shows that the half-filling condition $\langle n_{\uparrow} \rangle = 1/2$ is $I(0, 0) = I(1, 1)$, which can only be true when $\mu = 0$. When $\mu = 0$, the curves of $V(x)$ for $n = 0$ and $n = 2$ are reflections of each other in the y axis, thus giving us symmetry between the “hole” and “particle” curves.

A more formal analysis is to apply a particle-hole transformation (PHT), $d_{i\sigma} = (-1)^{i_x+i_y} c_{i\sigma}^{\dagger}$, on the Hamiltonian. This choice of alternating signs between different sublattices sites ensures that the electron hopping term remains the same under the PHT. Meanwhile, the density operator $n_{i\sigma}$ transforms into $1 - n_{i\sigma}$. If we also introduce $y_i = -x_i$ we see that the original Hamiltonian is recovered except for a change in sign of the chemical potential μ . This demonstrates that density of the system obeys $n(\mu) = 2 - n(-\mu)$. From this, it is obvious that $\mu = 0$ yields half-filling $n = \langle n_{i\uparrow} + n_{i\downarrow} \rangle = 1$.

Appendix 2: Relation between A and B to fix x_0

In order to compare results of simulations of the anharmonic model to the original Holstein Hamiltonian, setting the el-ph coupling λ and phonon frequency ω_0 (with $\omega_0 = \sqrt{2A}$) to be the same, as done in Sec. III, is not sufficient. The reason is that the electrons move in an energy landscape given by the *product* of λ and phonon displacement. A comparison which ensures equivalence of the energy landscape is obtained by requiring that λx_0 be the same in the double well potential as in the conventional Holstein model. Here x_0 is the position of the

minima in the phonon potential corresponding to empty ($n = 0$) and doubly occupied ($n = 2$) sites.

In the conventional Holstein Hamiltonian, at half-filling ($\mu = 0$)

$$V = \frac{1}{2}\omega_0^2 x^2 + \lambda x(n-1). \quad (7)$$

and the minima are at $x_0 = \pm\lambda/\omega_0^2$ for $n = 0$ and $n = 2$, respectively. It is straightforward to determine A, B in the anharmonic double well potential to give the same x_0 . The phonon potential is given by Eq. (4) with $\mu = 0$ at half-filling. The minimum of the $n = 0$ curve is at positive x_0 (the minimum for $n = 2$ being at $-x_0$) and given by the condition

$$-2Ax_0 + 4Bx_0^3 - \lambda = 0. \quad (8)$$

Therefore, to keep the locations of the minima fixed, A and B must satisfy

$$A = \frac{4Bx_0^3 - \lambda}{2x_0}. \quad (9)$$

In addition, one should use the same value of λ in both models so that the product λx_0 is the same. Thus in Sec. IV we proceed by fixing a (small) B and using Eq. 9 to determine A . Commonly used parameters are, for example, $\lambda = 2$ and $\omega_0 = 1$ which yield $x_0 = 2$. We used these parameters for comparison. We note that the height of the barrier at x_0 between the minima is given by $Ax_0^2 + Bx_0^4 - \lambda x_0$.

Appendix 3: Comparison of DQMC and Langevin Methods

The determinant quantum Monte Carlo (DQMC) and Langevin QMC algorithms differ in how they sample the fermion determinant. The partition function of the system is given by,

$$Z = \text{Tr} e^{-\beta H} \quad (10)$$

$$= \text{Tr} e^{-\Delta\tau H} e^{-\Delta\tau H} \dots e^{-\Delta\tau H}, \quad (11)$$

where H is given by Eq.(1), and $\Delta\tau$ is the imaginary time step, $\beta \equiv L_\tau \Delta\tau$. Complete sets of phonon coherent states, $\{x_{\vec{i},\tau}\}$ are inserted at each imaginary time slice which then allows us to express the trace over the phonon operators as a path integral. In addition, since the

fermion operators appear only in quadratic form, they can be traced out leading to the well known expression,⁵¹

$$\mathcal{Z} = \int \mathcal{D}x_{\vec{i},\tau} e^{-S_{\text{ph}}} [\det M(\{x_{\vec{i},\tau}\})]^2, \quad (12)$$

where the ‘‘phonon action’’ is

$$S_{\text{ph}} = \frac{\Delta\tau}{2} \left[\omega^2 \sum_{\vec{i}} x_{\vec{i},\tau}^2 + \sum_{\vec{i}} \left(\frac{x_{\vec{i},\tau+1} - x_{\vec{i},\tau}}{\Delta\tau} \right)^2 \right] \quad (13)$$

In DQMC, the statistical weight, the integrand in Eq.(12), is sampled directly by using the Metropolis update scheme: every site is visited and an attempt is made to change the phonon variable there. The attempted change is accepted or rejected using the Metropolis criterion.⁷⁴ In the Langevin approach,⁵⁵ the partition function is first written as,

$$\mathcal{Z} = \int \mathcal{D}x_{\vec{i},\tau} e^{-S}, \quad (14)$$

where

$$S = S_{\text{ph}} - \ln(\det M)^2. \quad (15)$$

Now the phonon field, $\{x_{\vec{i},\tau}\}$ is evolved using the Langevin equation which, in the simplest Euler discretized time form, is given by,⁵⁵

$$x_{\vec{i},\tau,t+dt} = x_{\vec{i},\tau,t} - dt \frac{\partial S}{\partial x_{\vec{i},\tau,t}} + \sqrt{2dt} \eta_{\vec{i},\tau,t}, \quad (16)$$

where t is the Langevin time, and η is a Gaussian distributed stochastic variable. In practice we use higher order Runge-Kutta discretization and, because the entire field is updated in one time step, we also use Fourier acceleration⁵⁵ which greatly reduces critical slowing down, speeding up convergence of configurations to equilibrium. Fourier acceleration cannot be used with DQMC because the field is updated one site at a time.

For more technical details, see Refs. 51, 75, and 76 for DQMC and Ref. 55 for Langevin.

Appendix 4: Visualization of Anharmonic Potentials

Throughout this paper, we discuss results from five different choices of the parameters A and B of the anharmonic potential given in Eq. (4) at $\mu = 0$. The first three choices, for common used parameters, are shown in Fig. 10. For visual simplicity, we show only the $n = 0$ and $n = 2$ curves for each parameter set.

We also show, in Fig. 11, the two potentials for the parameters that fix the average phonon displacement. Again only the $n = 0$ and $n = 2$ curves are shown for each parameter set. The minima are aligned, showing that x_0 is fixed at 2.

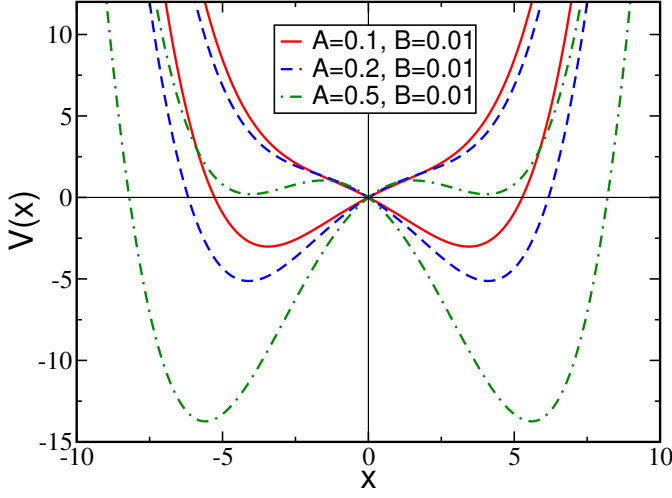


FIG. 10. (Color online). Plots of $V(x) = -Ax^2 + Bx^4 + \lambda x(n-1)$ for $n = 0$ and $n = 2$ for $(A, B) = (0.1, 0.01)$ [red, solid], $(0.2, 0.01)$ [blue, dashed], $(0.5, 0.01)$ [green, dotted dashed]. Here, $\lambda = \sqrt{2}\omega_0 g$, where $\omega_0 = \sqrt{2A}$ and $g = 1$.

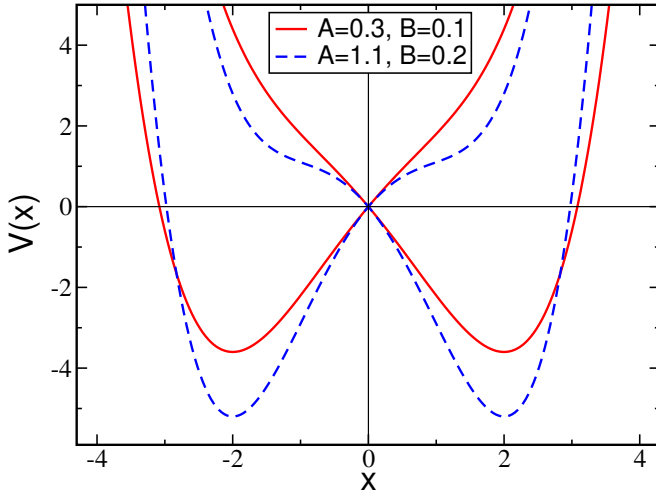


FIG. 11. (Color online). Plots of $V(x) = -Ax^2 + Bx^4 + \lambda x(n-1)$ for $n = 0$ and $n = 2$ for $(A, B) = (0.3, 0.1)$ [red, full line], and $(1.1, 0.2)$ [blue, dashed]. Here $\lambda = 2$ and $\omega_0 = 1$ to give $x_0 = 2$ for both parameter sets.

* Corresponding author: Claire.Kvande19@kzoo.edu

¹ Th. Holstein, “Studies of polaron motion: Part I. the molecular-crystal model,” *Ann. Phys. (N. Y.)* **8**, 325 (1959).

² PE Kornilovitch, “Continuous-time quantum Monte Carlo algorithm for the lattice polaron,” *Physical Review Letters* **81**, 5382 (1998).

³ PE Kornilovitch, “Ground-state dispersion and density of states from path-integral Monte Carlo: Application to the

lattice polaron,” *Physical Review B* **60**, 3237 (1999).

⁴ AS Alexandrov, “Polaron dynamics and bipolaron condensation in cuprates,” *Physical Review B* **61**, 12315 (2000).

⁵ Martin Hohenadler, Hans Gerd Evertz, and Wolfgang Von der Linden, “Quantum Monte Carlo and variational approaches to the Holstein model,” *Physical Review B* **69**, 024301 (2004).

⁶ Li-Chung Ku, SA Trugman, and Janez Bonča, “Dimensionality effects on the Holstein polaron,”

- Physical Review B **65**, 174306 (2002).
- 7 Paul E Spencer, JH Samson, PE Kornilovitch, and AS Alexandrov, “Effect of electron-phonon interaction range on lattice polaron dynamics: A continuous-time quantum Monte Carlo study,” *Physical Review B* **71**, 184310 (2005).
 - 8 Alexandru Macridin, GA Sawatzky, and Mark Jarrell, “Two-dimensional Hubbard-Holstein bipolaron,” *Physical Review B* **69**, 245111 (2004).
 - 9 Aldo H Romero, David W Brown, and Katja Lindenberg, “Effects of dimensionality and anisotropy on the Holstein polaron,” *Physical Review B* **60**, 14080 (1999).
 - 10 Janez Bonča, SA Trugman, and I Batistić, “Holstein polaron,” *Physical Review B* **60**, 1633 (1999).
 - 11 Rudolf Ernst Peierls, *Surprises in theoretical physics*, Vol. 107 (Princeton University Press, 1979).
 - 12 Jorge E Hirsch and Eduardo Fradkin, “Effect of quantum fluctuations on the Peierls instability: a Monte Carlo study,” *Physical Review Letters* **49**, 402 (1982).
 - 13 Jorge E Hirsch and Eduardo Fradkin, “Phase diagram of one-dimensional electron-phonon systems. ii. the molecular-crystal model,” *Physical Review B* **27**, 4302 (1983).
 - 14 R. T. Scalettar, N. E. Bickers, and D. J. Scalapino, “Competition of pairing and Peierls-charge-density-wave correlations in a two-dimensional electron-phonon model,” *Phys. Rev. B* **40**, 197 (1989).
 - 15 F. Marsiglio, “Pairing and charge-density-wave correlations in the Holstein model at half-filling,” *Phys. Rev. B* **42**, 2416 (1990).
 - 16 JK Freericks, M Jarrell, and DJ Scalapino, “Holstein model in infinite dimensions,” *Physical Review B* **48**, 6302 (1993).
 - 17 Takahiro Ohgoe and Masatoshi Imada, “Competition among superconducting, antiferromagnetic, and charge orders with intervention by phase separation in the 2d Holstein-Hubbard model,” *Physical Review Letters* **119**, 197001 (2017).
 - 18 M. Hohenadler and G.G. Batrouni, “Dominant charge density wave correlations in the Holstein model on the half-filled square lattice,” *Phys. Rev. B* **100**, 165114 (2019).
 - 19 Owen Bradley, George G. Batrouni, and Richard T. Scalettar, “Superconductivity and charge density wave order in the two-dimensional Holstein model,” *Phys. Rev. B* **103**, 235104 (2021).
 - 20 B. Noszarzewski, E. W. Huang, Philip M. Dee, I. Esterlis, B. Moritz, S. A. Kivelson, S. Johnston, and T. P. Devereaux, “Superconductivity, charge density waves, and bipolarons in the Holstein model,” *Phys. Rev. B* **103**, 235156 (2021).
 - 21 Maykon V. Araújo, José P. de Lima, Sandro Sorella, and Natanael C. Costa, “Two-dimensional $t - t'$ Holstein model,” *Phys. Rev. B* **105**, 165103 (2022).
 - 22 Stefan Blawid and Andrew J. Millis, “Quantum phonons and the charge-density-wave transition temperature: A dynamical mean-field study,” *Phys. Rev. B* **63**, 115114 (2001).
 - 23 M. Weber and M. Hohenadler, “Two-dimensional Holstein-Hubbard model: Critical temperature, Ising universality, and bipolaron liquid,” *Phys. Rev. B* **98**, 085405 (2018).
 - 24 Y.-X. Zhang, W.-T. Chiu, N.C. Costa, G.G. Batrouni, and R.T. Scalettar, “Charge order in the Holstein model on a honeycomb lattice,” *Phys. Rev. Lett.* **122**, 077602 (2019).
 - 25 C. Feng, H. Guo, and R. T. Scalettar, “Charge density waves on a half-filled decorated honeycomb lattice,” *Phys. Rev. B* **101**, 205103 (2020).
 - 26 C. Feng and R. T. Scalettar, “Interplay of flat electronic bands with Holstein phonons,” *Phys. Rev. B* **102**, 235152 (2020).
 - 27 C. Chen, X. Y. Xu, Z. Y. Meng, and M. Hohenadler, “Charge-density-wave transitions of Dirac fermions coupled to phonons,” *Phys. Rev. Lett.* **122**, 077601 (2019).
 - 28 B Cohen-Stead, K Barros, ZY Meng, C Chen, RT Scalettar, and GG Batrouni, “Langevin simulations of the half-filled cubic Holstein model,” *Phys. Rev. B* **102**, 161108 (2020).
 - 29 I Esterlis, SA Kivelson, and DJ Scalapino, “A bound on the superconducting transition temperature,” *npj Quantum Materials* **3**, 1–4 (2018).
 - 30 Bo Xing, Wei-Ting Chiu, Dario Poletti, R. T. Scalettar, and George Batrouni, “Quantum Monte Carlo simulations of the 2d Su-Schrieffer-Heeger model,” *Phys. Rev. Lett.* **126**, 017601 (2021).
 - 31 Chunhan Feng, Bo Xing, Dario Poletti, Richard Scalettar, and George Batrouni, “Phase diagram of the Su-Schrieffer-Heeger-Hubbard model on a square lattice,” *Phys. Rev. B* **106**, L081114 (2022).
 - 32 A. Götz, S. Beyl, M. Hohenadler, and F. F. Assaad, “Valence-bond solid to antiferromagnet transition in the two-dimensional Su-Schrieffer-Heeger model by Langevin dynamics,” *Phys. Rev. B* **105**, 085151 (2022).
 - 33 Xun Cai, Zi-Xiang Li, and Hong Yao, “Antiferromagnetism induced by bond Su-Schrieffer-Heeger electron-phonon coupling: A quantum Monte Carlo study,” *Phys. Rev. Lett.* **127**, 247203 (2021).
 - 34 John Sous, Monodeep Chakraborty, Roman V Krems, and Mona Berciu, “Light bipolarons stabilized by Peierls electron-phonon coupling,” *Physical Review Letters* **121**, 247001 (2018).
 - 35 C. Zhang, J. Sous, D. R. Reichman, M. Berciu, A. J. Millis, N. V. Prokof'ev, and B. V. Svistunov, “Bipolaronic high-temperature superconductivity,” *Phys. Rev. X* **13**, 011010 (2023).
 - 36 Benjamin Cohen-Stead, Kipton Barros, Richard Scalettar, and Steven Johnston, “A hybrid Monte Carlo study of bond-stretching electron-phonon interactions and charge order in the bismuthate family of superconductors,” *arXiv preprint arXiv:2208.02339* (2022).
 - 37 JK Freericks, M Jarrell, and GD Mahan, “The anharmonic electron-phonon problem,” *Physical Review Letters* **77**, 4588 (1996).
 - 38 A Chatterjee and Y Takada, “The Hubbard-Holstein model with anharmonic phonons in one dimension,” *J. Phys. Soc. Jap.* **73**, 964 (2004).
 - 39 CPJ Adolphs and M Berciu, “Going beyond the linear approximation in describing electron-phonon coupling: Relevance for the Holstein model,” *Europhysics Letters* **102**, 47003 (2013).
 - 40 S Li and S Johnston, “The effects of nonlinear electron-phonon interactions on superconductivity and charge-density-wave correlations,” *Europhysics Letters* **109**, 27007 (2015).
 - 41 S Li, EA Nowadnick, and S Johnston, “Quasiparticle properties of the nonlinear Holstein model at finite doping and temperature,” *Physical Review B* **92**, 064301 (2015).
 - 42 Philip M Dee, Jennifer Coulter, Kevin G Kleiner, and Steven Johnston, “Relative importance of nonlinear

- electron-phonon coupling and vertex corrections in the Holstein model,” *Communications Physics* **3**, 1–7 (2020).
- ⁴³ Ch Uma Lavanya, IV Sankar, and A Chatterjee, “Metallicity in a Holstein-Hubbard chain at half filling with Gaussian anharmonicity,” *Sci. Rep.* **7**, 3774 (2017).
- ⁴⁴ JCK Hui and PB Allen, “Effect of lattice anharmonicity on superconductivity,” *J. Phys. F* **4**, L42 (1974).
- ⁴⁵ AE Kavakozov and EG Maksimov, “Influence of anharmonicity on superconductivity,” *Sov. Phys. JETP* **47**, 358 (1978).
- ⁴⁶ GD Mahan and JO Sofo, “Resistivity and superconductivity from anharmonic phonons,” *Physical Review B* **47**, 8050 (1993).
- ⁴⁷ Attila Szabó, SA Parameswaran, and Sarang Gopalakrishnan, “High-temperature transport and polaron speciation in the anharmonic Holstein model,” *arXiv preprint arXiv:2110.10170* (2021).
- ⁴⁸ Jun Kondo, “Localized atomic states in metals,” *Physica B+ C* **84**, 40–49 (1976).
- ⁴⁹ Takahiro Fuse and Yoshiaki Ōno, “Rattling-induced heavy fermion state in the anharmonic Holstein model,” *Journal of the Physical Society of Japan* **80**, SA136 (2011).
- ⁵⁰ Takahiro Fuse, Yoshiaki Ōno, and Takashi Hotta, “Heavy-electron formation and polaron-bipolaron transition in the anharmonic Holstein model,” *Journal of the Physical Society of Japan* **81**, 044701 (2012).
- ⁵¹ R Blankenbecler, DJ Scalapino, and RL Sugar, “Monte Carlo calculations of coupled boson-fermion systems. i,” *Phys. Rev. D* **24**, 2278 (1981).
- ⁵² R. M. Noack and D. J. Scalapino, “Green’s-function self-energies in the two-dimensional holstein model,” *Phys. Rev. B* **47**, 305–308 (1993).
- ⁵³ M. Vekić, R.M. Noack, and S.R. White, “Charge-density waves versus superconductivity in the Holstein model with next-nearest-neighbor hopping,” *Phys. Rev. B* **46**, 271 (1992).
- ⁵⁴ F Marsiglio, “The spectral function of a one-dimensional Holstein polaron,” *Physics Letters A* **180**, 280–284 (1993).
- ⁵⁵ GG Batrouni and RT Scalettar, “Langevin simulations of a long range electron phonon model,” *Phys. Rev. B* **99**, 035114 (2019).
- ⁵⁶ G Paleari, F Hébert, B Cohen-Stead, K Barros, RT Scalettar, and GG Batrouni, “Quantum Monte carlo study of an anharmonic Holstein model,” *Phys. Rev. B* **103**, 195117 (2021).
- ⁵⁷ B Cohen-Stead, C Bradley, O Miles, GG Batrouni, RT Scalettar, and K Barros, “Fast and scalable quantum Monte Carlo simulations of electron-phonon models,” *Phys. Rev. E* **105**, 065302 (2022).
- ⁵⁸ Y Zhang, C Feng, R Mondaini, GG Batrouni, and RT Scalettar, “Charge singlets and orbital-selective charge density wave transitions,” *Phys. Rev. B* **106**, 115120 (2022).
- ⁵⁹ GG Batrouni, GR Katz, AS Kronfeld, GP Lepage, B Svetitsky, and KG Wilson, “Langevin simulations of lattice field theories,” *Phys. Rev. D* **32**, 2736 (1983).
- ⁶⁰ Chuang Chen, Xiao Yan Xu, Junwei Liu, George Batrouni, Richard Scalettar, and Zi Yang Meng, “Symmetry-enforced self-learning Monte Carlo method applied to the Holstein model,” *Phys. Rev. B* **98**, 041102 (2018).
- ⁶¹ Meng Yao, Da Wang, and Qiang-Hua Wang, “Reducing autocorrelation time in determinant quantum Monte Carlo using the Wang-Landau algorithm: Application to the Holstein model,” *Phys. Rev. E* **104**, 025305 (2021).
- ⁶² A.B. Migdal, “Interactions between electrons and lattice vibrations in a normal metal,” *Sov. Phys. JETP* **7**, 999 (1958).
- ⁶³ G.M. Eliashberg, “Interactions between electrons and lattice vibrations in a superconductor,” *Sov. Phys. JETP* **11**, 696 (1960).
- ⁶⁴ AS Alexandrov, “Breakdown of the migdal-eliasberg theory in the strong-coupling adiabatic regime,” *Europhysics Letters* **56**, 92 (2001).
- ⁶⁵ ED Bauer, Yi-feng Yang, C Capan, RR Urbano, CF Miclea, H Sakai, F Ronning, MJ Graf, AV Balatsky, R Movshovich, *et al.*, “Electronic inhomogeneity in a kondo lattice,” *Proceedings of the National Academy of Sciences* **108**, 6857–6861 (2011).
- ⁶⁶ Assa Auerbach and K. Levin, “Kondo bosons and the kondo lattice: Microscopic basis for the heavy fermi liquid,” *Phys. Rev. Lett.* **57**, 877–880 (1986).
- ⁶⁷ Hirokazu Tsunetsugu, Manfred Sigrist, and Kazuo Ueda, “The ground-state phase diagram of the one-dimensional kondo lattice model,” *Reviews of Modern Physics* **69**, 809 (1997).
- ⁶⁸ Frank Steglich and Steffen Wirth, “Foundations of heavy-fermion superconductivity: lattice kondo effect and mott physics,” *Reports on Progress in Physics* **79**, 084502 (2016).
- ⁶⁹ Melvin A Ruderman and Charles Kittel, “Indirect exchange coupling of nuclear magnetic moments by conduction electrons,” *Physical Review* **96**, 99 (1954).
- ⁷⁰ Tadao Kasuya, “A theory of metallic ferro- and antiferromagnetism on zener’s model,” *Progress of theoretical physics* **16**, 45–57 (1956).
- ⁷¹ Kei Yosida, “Magnetic properties of cu-mn alloys,” *Physical Review* **106**, 893 (1957).
- ⁷² Mogens Christensen, Asger B Abrahamsen, Niels B Christensen, Fanni Juranyi, Niels H Andersen, Kim Lefmann, Jakob Andreasson, Christian RH Bahl, and Bo B Iversen, “Avoided crossing of rattler modes in thermoelectric materials,” *Nature materials* **7**, 811–815 (2008).
- ⁷³ George S Nolas, Joe Poon, and Mercouri Kanatzidis, “Recent developments in bulk thermoelectric materials,” *MRS bulletin* **31**, 199–205 (2006).
- ⁷⁴ Nicholas Metropolis, Arianna W. Rosenbluth, Marshall N. Rosenbluth, Augusta H. Teller, and Edward Teller, “Equation of State Calculations by Fast Computing Machines,” *The Journal of Chemical Physics* **21**, 1087–1092 (2004).
- ⁷⁵ S. R. White, D. J. Scalapino, R. L. Sugar, E. Y. Loh, J. E. Gubernatis, and R. T. Scalettar, “Numerical study of the two-dimensional hubbard model,” *Phys. Rev. B* **40**, 506–516 (1989).
- ⁷⁶ F.F. Assaad and H.G. Evertz, “World-line and determinantal quantum monte carlo methods for spins, phonons and electrons,” in *Computational Many-Particle Physics*, edited by H. Fehske, R. Schneider, and A. Weiße (Springer Berlin Heidelberg, Berlin, Heidelberg, 2008) pp. 277–356.